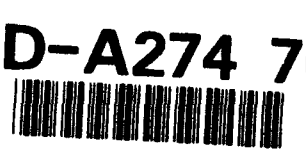

AD

TECHNICAL REPORT ARCCB-TR-93038

POWER LAWS, FLICKER NOISE, AND THE BARKHAUSEN EFFECT

L.V. MEISEL
P.J. COTE

OCTOBER 1993

US ARMY ARMAMENT RESEARCH,
DEVELOPMENT AND ENGINEERING CENTER
CLOSE COMBAT ARMAMENTS CENTER
BENÉT LABORATORIES
WATERVLIET, N.Y. 12189-4050

APPROVED FOR PUBLIC RELEASE; DISTRIBUTION UNLIMITED

DISCLAIMER

The findings in this report are not to be construed as an official Department of the Army position unless so designated by other authorized documents.

The use of trade name(s) and/or manufacturer(s) does not constitute an official indorsement or approval.

DESTRUCTION NOTICE

For classified documents, follow the procedures in DoD 5200.22-M, Industrial Security Manual, Section II-19 or DoD 5200.1-R, Information Security Program Regulation, Chapter IX.

For unclassified, limited documents, destroy by any method that will prevent disclosure of contents or reconstruction of the document.

For unclassified, unlimited documents, destroy when the report is no longer needed. Do not return it to the originator.

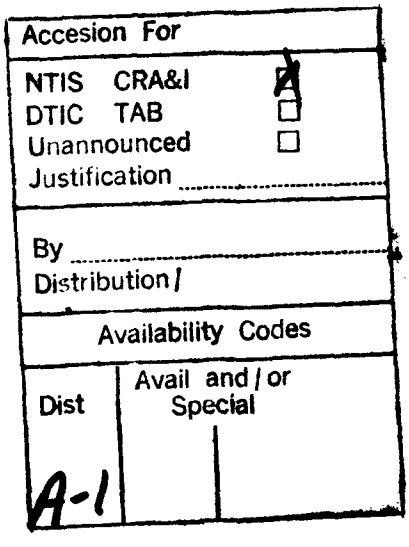

REPORT DOCUMENTATION PAGE

Form Approved
OMB No. 0704-0188

1. AGENCY USE ONLY *(Leave blank)*	2. REPORT DATE	3. REPORT TYPE AND DATES COVERED
	October 1993	Final

4. TITLE AND SUBTITLE
POWER LAWS, FLICKER NOISE, AND THE BARKHAUSEN EFFECT

5. FUNDING NUMBERS
AMCMS: 6111.02.H611.1

6. AUTHOR(S)
L.V. Meisel and P.J. Cote

7. PERFORMING ORGANIZATION NAME(S) AND ADDRESS(ES)
U.S. Army ARDEC
Benét Laboratories, SMCAR-CCB-TL
Watervliet, NY 12189-4050

8. PERFORMING ORGANIZATION REPORT NUMBER
ARCCB-TR-93038

9. SPONSORING / MONITORING AGENCY NAME(S) AND ADDRESS(ES)
U.S. Army ARDEC
Close Combat Armaments Center
Picatinny Arsenal, NJ 07806-5000

10. SPONSORING / MONITORING AGENCY REPORT NUMBER

11. SUPPLEMENTARY NOTES
Published in *Physical Review B*

12a. DISTRIBUTION / AVAILABILITY STATEMENT
Approved for public release; distribution unlimited

12b. DISTRIBUTION CODE

13. ABSTRACT *(Maximum 200 words)*

The Barkhausen effect was studied in three ferromagnetic metals: an amorphous alloy, iron, and alumel. The data exhibit all the characteristics of self-organized critical behavior enumerated by Bak, Tang, and Weisenfeld: The distributions of pulse durations, areas, and energies have the form of power laws, which have been modified to account for finite-size effects as suggested by Kadanoff, Nagel, Wu, and Zhou, and the power spectral densities have the form of flicker noise. Furthermore, the parameters describing the Barkhausen noise pulse distributions are consistent with those characterizing the power spectral density in the light of the results of Jensen, Christensen, and Fogedby. The data are also consistent with a model based on an inherent static fractal structure, independent of a self-organizing principle.

14. SUBJECT TERMS
Barkhausen Effect, Self-Organized Criticality, Power-Law Distributions, Flicker Noise, Ferromagnetism, Amorphous Metal

15. NUMBER OF PAGES
19

16. PRICE CODE

17. SECURITY CLASSIFICATION OF REPORT	18. SECURITY CLASSIFICATION OF THIS PAGE	19. SECURITY CLASSIFICATION OF ABSTRACT	20. LIMITATION OF ABSTRACT
UNCLASSIFIED	UNCLASSIFIED	UNCLASSIFIED	UL

TABLE OF CONTENTS

List of Illustrations

INTRODUCTION

Bak, Tang, and Weisenfeld (ref 1) (BTW) introduced the concept of self-organized criticality (SOC) to provide a consistent explanation for the fractal spatial structures, power-law distributions, and flicker noise commonly observed in spatially extended, dissipative, dynamical systems. Jensen, Christensen, and Fogedby (ref 2) (JCF) clarified the ideas in BTW and established the connection between the power-law dependencies and the power spectral densities. The consequences of the SOC concept have been extensively explored through computer simulations of sandpile dynamics (refs 1-4) and earthquake phenomena (refs 5,6).

The most striking application of the theory describes the state of the earth's crust as a self-organized critical system and provides a basis for understanding the Gutenberg-Richter law for the distribution of earthquake magnitudes (ref 5). There is also a growing body of experimental investigations of SOC-related phenomena including studies of actual sandpile dynamics (refs 7,8), motion of magnetic domains in garnet films (ref 9), sliding friction (ref 10), and the Barkhausen effect in glassy metals (ref 11).

The Barkhausen effect is a natural candidate for the SOC concept. The magnetic response of a ferromagnet is determined by its initial magnetic domain distribution and its response to applied magnetic fields.

For small fields, kinetic barriers permit only small reversible domain-wall motions, and the system remains magnetically elastic in analogy with elastic-plastic deformation or slip-stick SOC earthquake models (ref 5). As the applied field approaches and exceeds the magnitude of the coercive force, the specimen magnetization increases rapidly. The transition region is characterized by random irreversible domain-wall jumps and clusters of jumps analogous to slip in solids (e.g., in the earth's crust) when the applied force exceeds the yield strength and produces rapid, steplike increases in strain.

The stochastic character of domain-wall jumps, which is analogous to a mechanical slip in solids, arises from the complex patterns of local magnetic fields, internal stresses, and bulk and surface defects in ferromagnetic alloys. The fingerprint of SOC behavior is detected in the Barkhausen noise spectrum, which generally exhibits the f^{ε} dependence (ref 12) characteristic of SOC phenomena.

The present study refines the analysis of the Barkhausen effect in glassy metals (ref 11) and extends it to the Barkhausen effect in crystalline ferromagnets. In particular, the role of composition and microstructure on the Barkhausen effect was investigated by analysis of three different ferromagnetic materials: a glassy metal, iron, and alumel.

Measurements in the three ferromagnetic materials are consistent with the behavior of a self-organized critical system. The distributions of pulse energy releases for the three materials are remarkably well described by a power-law analogous to the Gutenberg-Richter law. Further, the Barkhausen pulse distributions from the three specimens exhibit a cutoff on pulse duration (size effect) that correlates with the presence of internal defects such as grain boundaries.

SAMPLE DESCRIPTION AND PREPARATION

We report on Barkhausen noise in three ferromagnetic metals:

1. Metglas 2605S ($Fe_{78}B_{13}Si_9$). The nominally 2-mil thick Metglas ribbon, supplied by Allied Signal, was cut into 2-mm by 20-mm samples, which were subsequently annealed for 15 minutes at 350°C to relieve residual stresses from the cutting process.

In some cases, highly reproducible peaks uncharacteristic of the general random behavior of the pulse trains were observed. The presence of the large reproducible peaks, however, did not significantly affect the results of the pulse analysis in those trials where they were detected. Annealing at $T \geq 400$°C, which completely relieves the internal stresses, was impractical since the Barkhausen peak amplitudes were reduced to such an extent that they could not be reliably distinguished.

These observations are consistent with the behavior of domain structures in 2605S studied by Livingston and Morris (ref 13). In the as-cast state, there is a wide distribution of domain sizes and types (in the unsaturated condition) generated by stresses from a variety of defects. At the other extreme--the fully annealed state--the stresses are greatly reduced, producing only a few large domains that tend to orient along the long axis of the specimen. In this condition, the permeability is at a maximum because the domain walls encounter much smaller resistances and the corresponding Barkhausen pulses are smaller and more difficult to detect. It should be noted that, except for the highly reproducible large amplitude pulses described above, no major differences were observed in the original (ref 11) and current studies of distributions of Barkhausen pulses from as-cast or partially annealed specimens.

2. Iron. Polycrystalline 5-mil iron thermocouple wire, provided by Omega Engineering, was cut into approximately 5-cm long specimens. Grain size was approximately 10μ.

3. Alumel ($Ni_{95}Al_3Mn_2$). Polycrystalline 5-mil alumel thermocouple wire, provided by Omega Engineering, was cut into approximately 5-cm long specimens. Mean grain size was approximately 10μ, however, in contrast to the iron specimen, the grains showed evidence of annealing twins in a light microscope, which is effectively a further subdivision of the grains. The density of annealing twins generally increases with the amount of prior deformation, which was necessarily large with the drawing of 5-mil wire.

Unlike Metglas, which has no grain boundaries in the amorphous state, the grain boundaries in polycrystalline metals represent a limit on the maximum size of the domains. In contrast to Metglas, where cutting or deformation can generate large amplitude Barkhausen pulses, mechanical deformation and surface abrasion of the polycrystalline specimens produced no dramatic changes in the character of the trains.

It also should be noted that the number of measurable Barkhausen pulses in the alumel specimen is relatively low and is sensitive to position along the wire, so that specimen has to be carefully positioned within the pickup coil to register a sufficiently large number of observable pulses within a given train for analysis.

THEORY

The salient idea in the theory of self-organized criticality as conceived by BTW is that extended dissipative dynamical systems tend to organize themselves into a critical state where chain reactions of *all* sizes in time and space propagate through the system. The absence of characteristic length and time scales in the SOC state imply fractal structure and "1/*f*" (or flicker) noise power spectral density. A collateral consequence of SOC is power-law dependencies (hyperbolic distributions) of energies released, chain reaction lifetimes, and cluster sizes. Thus, SOC provides a coherent basis for the common observation of power laws, 1/*f* noise, and fractal structure in nature.

Jensen, Christensen, and Fogedby (ref 2) clarified the results in BTW and explicitly revealed the important connection between power-law dependencies and power spectral density described by BTW. Kadanoff, Nagel, Wu, and Zhou (ref 3) extended the SOC concept to systems of finite extent.

JCF derive an expression for the power spectral density of a train of pulses that represent the chain reactions in an SOC system. JCF demonstrate that the power spectral density can be expressed as

$$S(f) = \frac{r}{(\pi f)^2} \int_0^\infty d\tau G(\tau)\sin^2(2\pi f\tau) \tag{1}$$

where r is the pulse repetition rate and $G(T)$ is a weighted distribution of lifetimes, defined as

$$G(T) = \int_0^\infty dA\, P(A,T)\, [A/T]^2 \tag{2}$$

where $P(A,T)$ is the joint probability for a pulse to have area A *and* length T.

JCF argue that if

$$G(T) \propto T^{\alpha}\exp(-T/T_0) \quad for\ t_0 \le T \le \infty\ , \tag{3}$$

then

$$for\ 1/T_0 \le f \le 1/t_0\ ,\ S(f) \approx const\ when\ \alpha < -3\ , \tag{4a}$$

$$for\ 1/T_0 \le f \le 1/t_0\ ,\ S(f) \propto f^{-(3+\alpha)}\ when\ -3 < \alpha < -1\ , \tag{4b}$$

$$for 1/T_0 \le f \le 1/t_0\ ,\ S(f) \propto f^{-2}\ when\ a > -1\ , \tag{4c}$$

$$for\ f \le 1/T_0\ ,\ S(f) \approx const\ , \tag{4d}$$

and

$$for\ 1/t_0 \le f\ ,\ S(f) \propto f^{-2}\ . \tag{4e}$$

We find that essentially the same results are obtained if

$$G(T) \propto T^{\alpha}H(T_c-T) \tag{3'}$$

where $H(x)$ is the Heaviside function, and the "cutoff pulse length" T_c plays the role of T_0. We refer to $1/T_c$ or $1/T_0$, which defines the break in Eq. (4) as the "transition frequency."

APPROACH

The two parts to our approach are as follows:

1. Measure the joint distribution functions $P_L[\ln(A),\ln(T)]$ for logarithmically-spaced bins. Linearly-spaced bins are not employed because the resulting histograms would contain only a few percent of the data outside the first bin. Thus, for linearly-spaced bins, the parameters of interest are determined by only a small fraction of the data, which represent ranges of pulse length where "size effects" are dominant and statistical significance is low.

The joint distribution functions $P(A,T)$, which appear in Eq. (2), are related to the measured logarithmic joint distribution functions as follows:

$$\begin{aligned} P(A,T)\ dA\ dT &= P_L[\ln(A),\ln(T)]\ d[\ln(A)]\ d[\ln(T)] \\ &= \{P_L[\ln(A),\ln(T)]/(AT)\}\ dA\ dT\ , \end{aligned}$$

which implies that

$$P(A,T) = P_L[\ln(A),\ln(T)]/(AT)\ . \tag{5}$$

- Integrate $P_L[\ln(A),\ln(T)]$ to obtain the log-spaced distribution functions $n_L[\ln(T)]$ and $n_L[\ln(A)]$. Investigate the suitability of hyperbolic distribution functions to describe $n_L[\ln(T)]$ and $n_L[\ln(A)]$. (The same notation is employed for different functions. Hopefully, no confusion will arise.)

Relationships analogous to Eq. (5) can be established between the log-spaced distribution functions and their linear-spaced counterparts $n(T)$ and $n(A)$. It is apparent that hyperbolic distribution of $n_L[\ln(x)]$ implies a hyperbolic distribution of $n(x)$ with exponent reduced by unity.

- Compute $G(T)$ via Eq. (2). Investigate the suitability of hyperbolic distribution functions and "size effect" forms to describe $G(T)$. Use the JCF rules, i.e., Eq. (4) to deduce the exponent and transition frequency in the power spectral density.

2. Employ Fast Fourier transform (FFT) and the Wiener-Khintchine theorem to deduce the power spectral density directly from Barkhausen noise signals. Determine exponents and transition frequencies and compare with the JCF computed results.

EXPERIMENTAL PROCEDURES

The sample is positioned within a pickup coil and the assembly is placed within an air-core solenoid. A signal generator provides a sinusoidal current to the solenoid, which produces a field that continuously drives the specimen through a *B-H* loop. The pickup coil detects the random, steplike changes in sample magnetization, and the data are amplified and recorded on a digital oscilloscope. The magnitude and frequency of the driving field are adjusted to minimize pulse overlap, while maintaining a sufficiently large number of pulses for meaningful analysis.

The air-core solenoid, which is comprised of numerous turns of 10-mil copper wire, is 5 cm long and 1 cm in diameter. The pickup coil, which comprises 200 turns of 5-mil copper wire, is 10 mm long and 3 mm in diameter. Generally, the driving field magnitude was maintained at less than 1 Oe and its frequency at less than 1 Hz. The signal from the pickup coil was amplified with a gain of 5000 through a Stanford Research System's low noise preamplifier with the bandwidth set at 0.3 to 30 kHz.

Typically, trains of several hundred Barkhausen pulses were selected at random and captured on a Nicolet digital oscilloscope, which recorded 4000 values per train. Sampling rates were selected to minimize aliasing effects on power spectra calculated via FFT; typical sampling rates were 5 to 10 μsec per point.

NUMERICAL PROCEDURES

Procedures for defining individual peaks and determining their distributions in Metglas 2605S, iron, and alumel were as follows:

1. A polynomial baseline, generally a cubic, is fit through minima on twenty equally-spaced intervals on each train. The signal level is then defined as the measured level minus the baseline.

2. The median signal level in a train is selected as a pulse-defining critical signal level. The critical signal level defined in this way lies just above the background noise and passes through the apparent base of the pulses and generally yields results consistent with less quantitative intuitive selection of peaks on the digital scope.

A typical train and its cubic baseline are shown in Figure 1. An expanded section from the same train, shown in Figure 2, illustrates the separation of major peaks.

3. The joint distribution function for logarithmically-spaced bins in pulse area A and length T, $P_L[\ln(A),\ln(T)]$, is measured for pulses defined as described above.

4. The measured $P_L[\ln(A),\ln(T)]$ were numerically integrated to obtain the distribution functions $n_L[\ln(A)]$ and $n_L[\ln(T)]$ and the JCF weighted density of states $G(T)$.

5. Power spectral densities $S(f)$ were computed by numerical integration based on the deduced $G(T)$.

6. Power spectral densities were determined directly from the pulse train data by means of FFT and the Wiener-Khintchine theorem.

7. Pulse energies were computed by numerical integration of the square of the measured voltages. We assume that these computed energies are approximately proportional to the energy released in a Barkhausen pulse.

MATLAB™ was used for all computations.

RESULTS

Figure 3 is a log-log plot of the pulse area versus pulse duration for a 297 pulse train of Barkhausen pulses for the iron specimen. Similar results are obtained with Metglas and alumel. Linear regression through all the points gives a slope of 1.4. Essentially the same value is obtained in Metglas and alumel and was measured in a previous study (ref 11) of Metglas 2605S.

Figures 4, 5, and 6 are log-log plots of the distribution of the 297 pulse durations, areas, and energies for iron. The data reflect power-law distributions with exponents -1.64, -1.88, and -1.44, respectively.

Figure 7 shows a log-log plot of the computed values of the JCF weighted distribution of pulse lifetimes $G(T)$ for the iron data. The slope of the linear portion of the graph is -1.0. Essentially the same exponent is found for alumel and Metglas.

Figure 8 shows a log-log plot of $S(f)$ computed via pulse analysis and FFT for the iron specimen. Both curves exhibit a transition to approximately f^2 for $f > 500$ Hz. The f^2 dependence is consistent with the $T^1H(T-T_o)$ form for $G(T)$.

Figures 9, 10, and 11 are log-log plots of the distributions of 137 pulse durations, areas, and energies for the alumel specimen. The corresponding power-law exponents are -2.1, -1.78, and -1.58, respectively.

Figure 12 shows the computed pulse and FFT results for alumel. Both show a transition to approximately f^2 for $f > 2000$ Hz. The difference in transition frequencies for iron and alumel are consistent with the differences in cutoff values for pulse durations as can be inferred from Figures 4 and 9.

Figures 13, 14, and 15 are log-log plots of distributions of durations, areas, and energies of 218 pulses for the Metglas sample. The corresponding power-law exponents are -1.82, -1.74, and -1.60, respectively. Earlier results (ref 11) on Metglas gave -2.26 rather than -1.81 for the duration exponent. The discrepancy (which is less than 1.3 σ from Reference 11) results from fitting to the sharp cutoff functional form with logarithmic binning rather than to the exponential cutoff form of JCF with linear binning as in Reference 11. The new result is believed to be more reliable.

Figure 16 shows the agreement between the computed pulse and FFT results for $S(f)$ for the Metglas sample. Both show a transition to approximately f^2 for $f > 1000$ Hz. The earlier result for the FFT computed $S(f)$ exponent was -1.244 (ref 11). We now believe that aliasing biased those data to produce the smaller exponent.

DISCUSSION

Pulse Distribution Analysis

Since hyperbolically-distributed data tend to be intensely concentrated at small sizes, logarithmically-spaced binning has proved to be better suited to fitting the data than conventional linearly-spaced binning. The problem with linear binning is that the fitting parameters (i.e., the exponents) are largely determined by the occupation values for low probability bins. Employing the techniques described in the Numerical Procedures section, i.e., log-spaced binning, the situation is dramatically improved. The problems in fitting reported in Reference 11 could have been largely resolved by employing logarithmically-spaced binning.

The Functional Form of the Pulse Distribution Data

The Exponential Cutoff Pulse Distribution Form of JCF

As noted in our earlier report on Metglas (ref 11), which fit the Barkhausen pulse distributions to a power law with *exponential cutoff*, the data appear to cut off faster than $\exp(-T/T_0)$.

Sharp Cutoff Pulse Distribution

The present pulse distributions and the earlier data are well approximated by hyperbolic distributions with a *sharp cutoff*, i.e.,

$$n(T) = F\ T^a\ H(T_c - T) \qquad (6)$$

where $H(x)$ is the Heaviside function and F is a constant as in Eq. (3'). The cutoff pulse duration T_c plays the role that T_0 plays in the exponential cutoff form in determining the frequency at which the transition to f^ε behavior in the power spectral density occurs. The differences in T_c as determined from the analysis of the Barkhausen pulse distributions in Metglas 2605S, iron, and alumel are reflected in the crossover frequencies in their power spectral densities.

Physical Interpretation of T_0 or T_c

The origin of cutoffs in SOC avalanche models is determined by the size of the model which imposes an upper limit on the size of avalanches. However, the present experimental data are consistent with the view that internal defects rather than external dimensions determine the cutoff on the size of the Barkhausen avalanches.

- Polycrystalline samples. The cutoff pulse size T_c correlates with grain size in the polycrystalline samples. The metallographically-determined grain structure is finer in the alumel wire (considering the subgrain annealing twins) than in the iron wire samples. Thus, as observed, the maximum domain size and largest avalanche would be expected to be smaller in the alumel wire.

- Amorphous samples. The situation is different in the Metglas 2605S samples. There are no grain boundaries. Furthermore, the domains in the Metglas ribbons are essentially two-dimensional and extend from the top to the bottom surfaces (ref 13). (The ribbon thickness was nonuniform and ranged from 1 to 2 mils in our samples.) The defects that limit the maximum size of domain jumps in the amorphous ribbons are expected to be internal stresses and surface imperfections produced during the rapid solidification process or subsequent treatment. The cutoffs are also consistent with the existence of

self-organized subcritical states as in the magnetic domain pattern studies of Bak and Flyvbjerg (ref 14).

The Korcak Law

The "area-number relations" are discussed by Mandelbrot (ref 15) in terms of the number of pulses whose area A exceeds a, denoted $N(A > a)$, which is related to the pulse distribution by

$$N(A>a) \equiv \int_a^\infty n(A)dA \ . \tag{7}$$

For hyperbolic distribution functions, $n(A) \approx n(1)\, A^{-q}$ with q a positive constant,

$$N(A>a) \approx n(1)\int_a^\infty A^{-q}dA = n(1)a^{-(q-1)}/(q-1) = Fa^{-B} \ , \tag{8}$$

i.e., the number of pulses whose area exceeds a will also be hyperbolically distributed if $B = q - 1 > 0$. Mandelbrot refers to the hyperbolic form of area-number relations as the Korcak law.

Universality

Despite substantial differences in domain sizes and configurations, the pulse distributions and power spectra measured in Metglas 2605S, iron, and alumel are strikingly similar. The only substantive differences in the Barkhausen data for the three materials are manifested in variations in the pulse cutoff values T_c and the corresponding limiting frequencies for the f^E behavior in the power spectral density.

Barkhausen Effect as a Manifestation of SOC

The theory of self-organized critical behavior described in BTW provides a fresh perspective on Barkhausen phenomena. The power-law distributions (hyperbolic distributions) and flicker noise, which are the hallmark of SOC, are conspicuous in Barkhausen phenomena. Furthermore, the quantitative link between the exponents characterizing the pulse distribution and the flicker noise in the power spectral density established by JCF for SOC systems holds for the present Barkhausen results.

The BTW theory of SOC phenomena provides a dynamical basis for the occurrence of hyperbolic distributions and the concomitant flicker noise. Therefore, the present Barkhausen data are consistent with SOC concepts concerning power-law distributions in dissipative dynamical systems.

Barkhausen Effect Reflecting Scale Invariant Static Structure

As Mandelbrot has stressed (ref 15), hyperbolic distributions are found in diverse scale invariant systems. Thus, inherent static structural features in Barkhausen systems, e.g., fragmentation or fractal grain or domain structure, independent of a self-organizing principle could yield the observed hyperbolic distributions of Barkhausen avalanche sizes.

A similar interpretation has been proposed for earthquake data. There is some evidence (refs 16,17) that the power-law distributions of earthquake magnitudes are a consequence of a power-law distribution of individual fault dimensions rather than a power-law distribution of earthquake sizes on a given fault. We plan to explore this possibility for the Barkhausen effect.

REFERENCES

1. P. Bak, C. Tang, and K. Weisenfeld, *Phys. Rev. Lett.*, Vol. 59, 1987, p. 381; *Phys. Rev. A*, Vol. 38, 1988, p. 36.

2. H.J. Jensen, K.C. Christensen, and H.C. Fogedby, *Phys. Rev. B*, Vol. 40, 1989, p. 7425.

3. L.P. Kadanoff, S.R. Nagel, L. Wu, and S-M. Zhou, *Phys. Rev. A*, Vol. 39, 1989, p. 6524.

4. C.P.C. Prado and Z. Olami, *Phys. Rev. A*, Vol. 45, 1992, p. 665.

5. K. Chen, P. Bak, and S.P. Obukhov, *Phys. Rev. A*, Vol. 43, 1991, p. 625.

6. See, for example, J. Lomnitz-Alder, L. Knopoff, and G. Martinez-Mekler, *Phys. Rev. A*, Vol. 45, 1992, p. 2211; Z. Olami, H.J.S. Feder, and K. Christensen, *Phys. Rev. Lett.*, Vol. 68, 1992, p. 1244; G. Ekstrom and A.M. Dziewonski, *Nature* (London), Vol. 332, 1988, p. 319.

7. G.A. Held, D.H. Solina II, D.T. Keane, W.J. Haag, P.M. Horn, and G. Grinstein, *Phys. Rev. Lett.*, Vol. 65, 1990, p. 1120.

8. H.M. Jaeger, C-H. Liu, and S.R. Nagel, *Phys. Rev. Lett.*, Vol. 62, 1989, p. 40.

9. K.L. Babcock and R.M. Westervelt, *Phys. Rev. Lett.*, Vol. 64, 1990, p. 2168.

10. H.J.S. Feder and J. Feder, *Phys. Rev. Lett.*, Vol. 66, 1991, p. 2669.

11. P.J. Cote and L.V. Meisel, *Phys. Rev. Lett.*, Vol. 67, 1991, p. 1334.

12. See for example, B. Alessandro, C. Beatrice, G. Bertotti, and A. Montorsi, *J. Appl. Phys.*, Vol. 68, 1990, p. 2908; H. Bittel, *IEEE Trans. Magn.*, Vol. 5, 1969, p. 359.

13. J.D. Livingston and W.G. Morris, *J. Appl. Phys.*, Vol. 57, 1985, p. 3555.

14. P. Bak and H. Flyvbjerg, *Phys. Rev. A*, Vol. 45, 1992, p. 2192.

15. B.B. Mandelbrot, *The Fractal Geometry of Nature*, Freeman, New York, 1983.

16. A.C. Johnston and S.J. Nava, *J. Geophys. Res.*, Vol. 90, 1985, p. 6737.

17. S.G. Wesnoushy, C.H. Scholz, K. Shimazaki, and T. Matsuda, *J. Geophys. Res.*, Vol. 88, 1983, p. 9331.

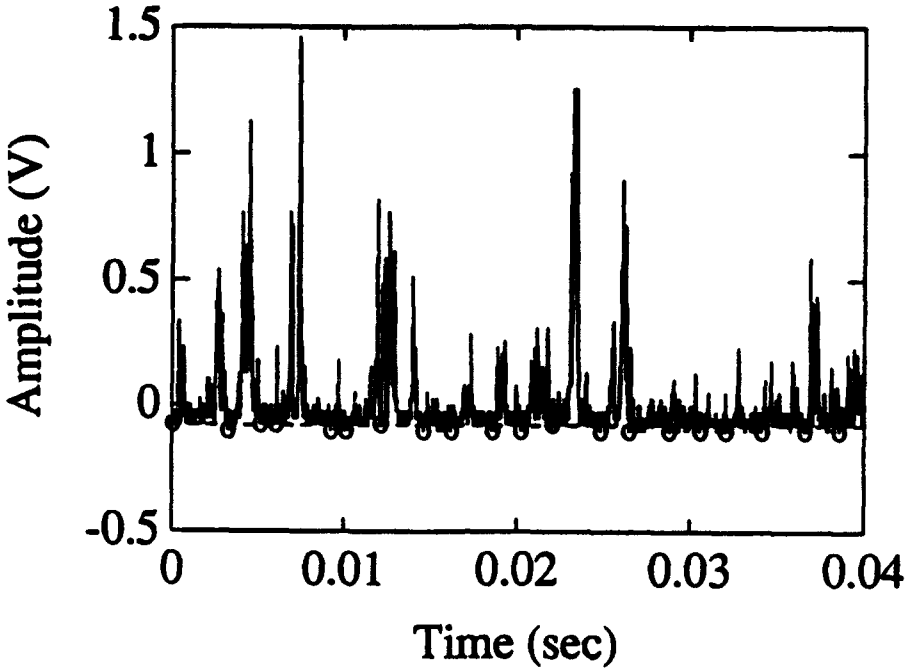

Figure 1. A typical Barkhausen pulse train for the iron specimen and a third-order polynomial baseline.

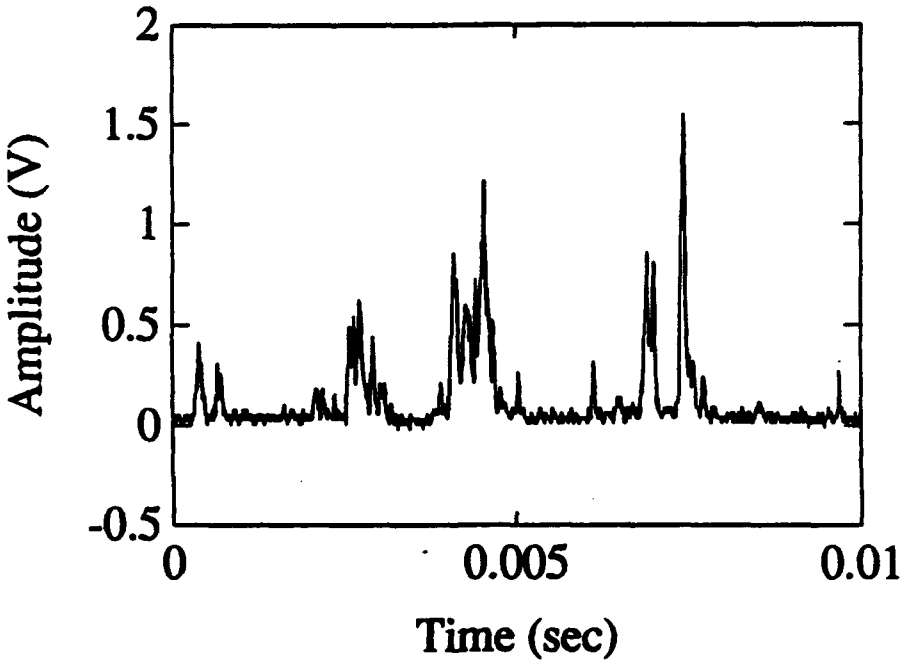

Figure 2. An expanded section of the Barkhausen pulse train of Figure 1 illustrating the separation of the major peaks.

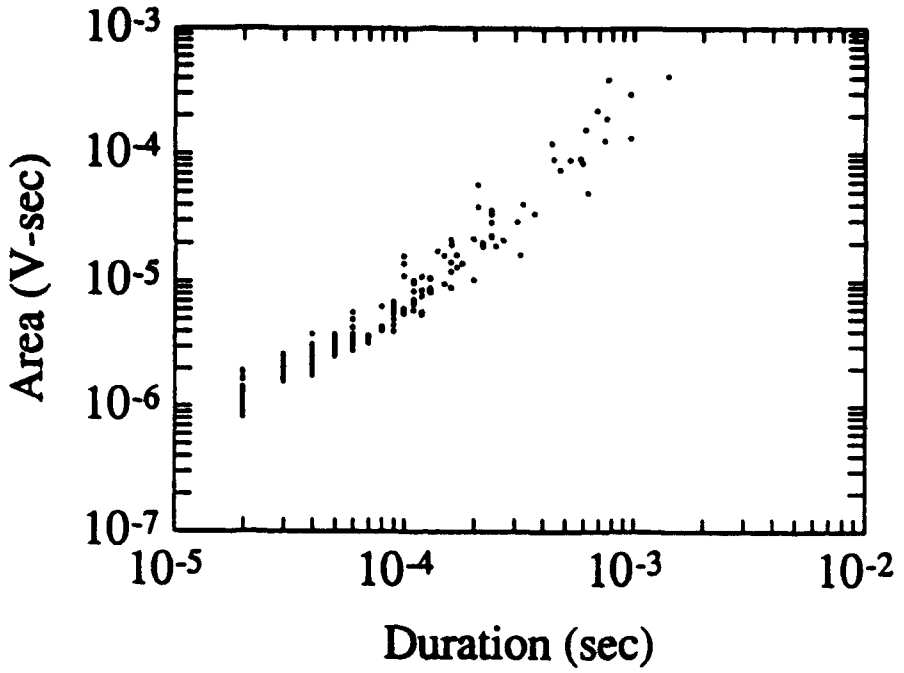

Figure 3. Pulse area versus pulse duration for a train of 297 Barkhausen pulses in the iron specimen.

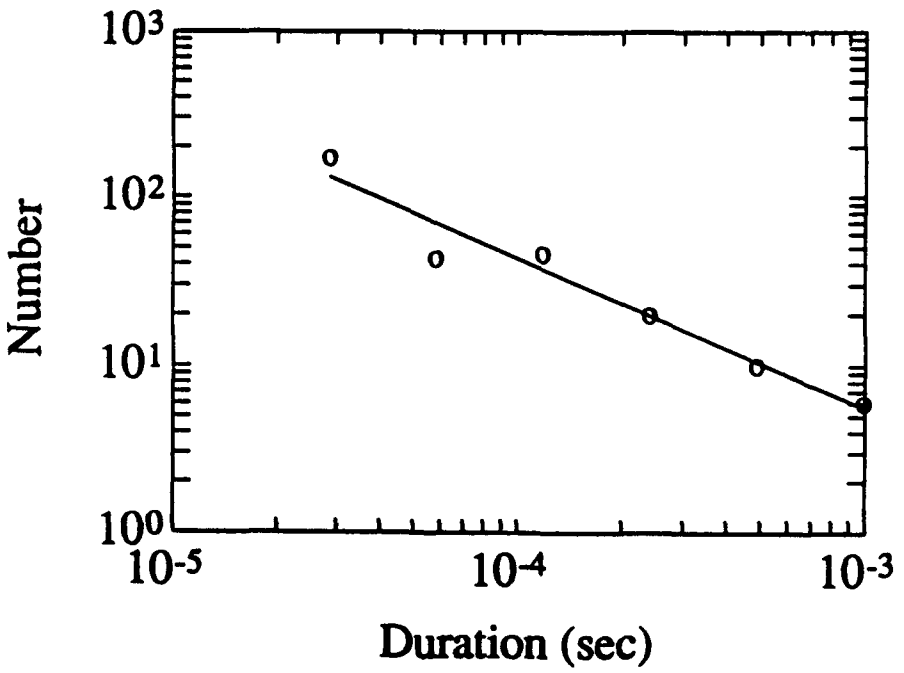

Figure 4. Distribution of pulse durations for the train of Figure 3.

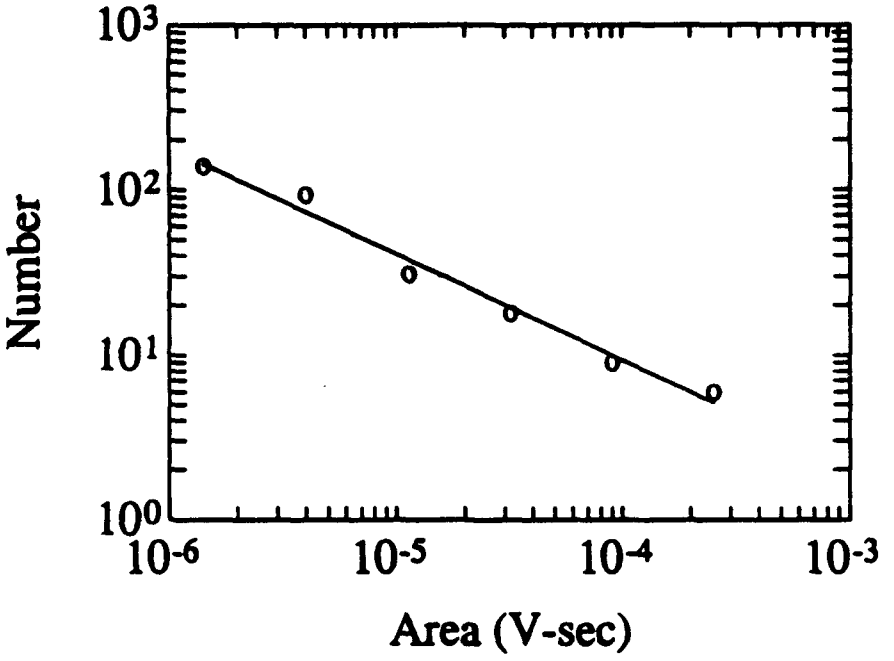

Figure 5. Distribution of areas for the train of Figure 3.

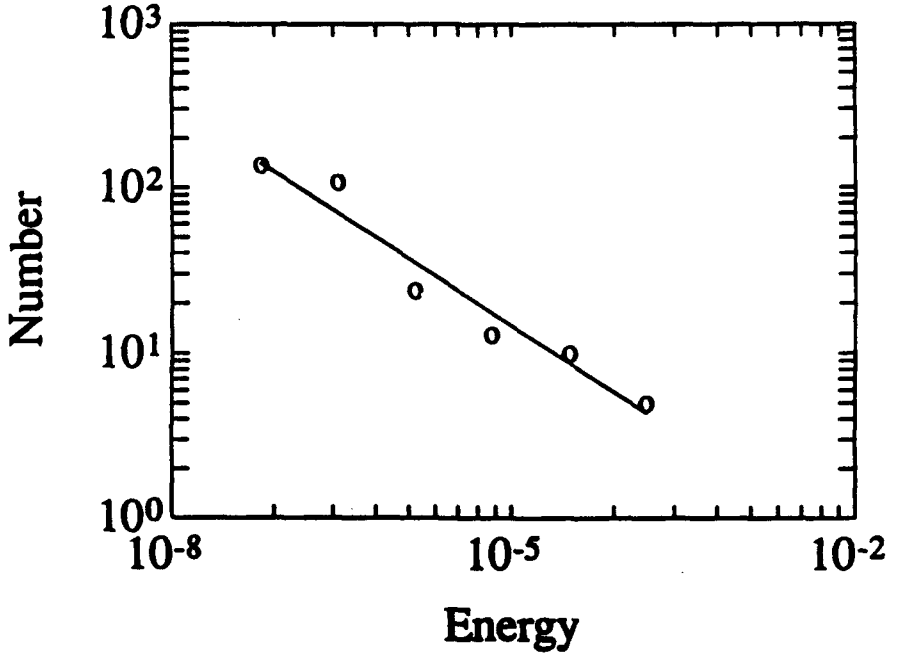

Figure 6. Distribution of energies for the train of Figure 3.

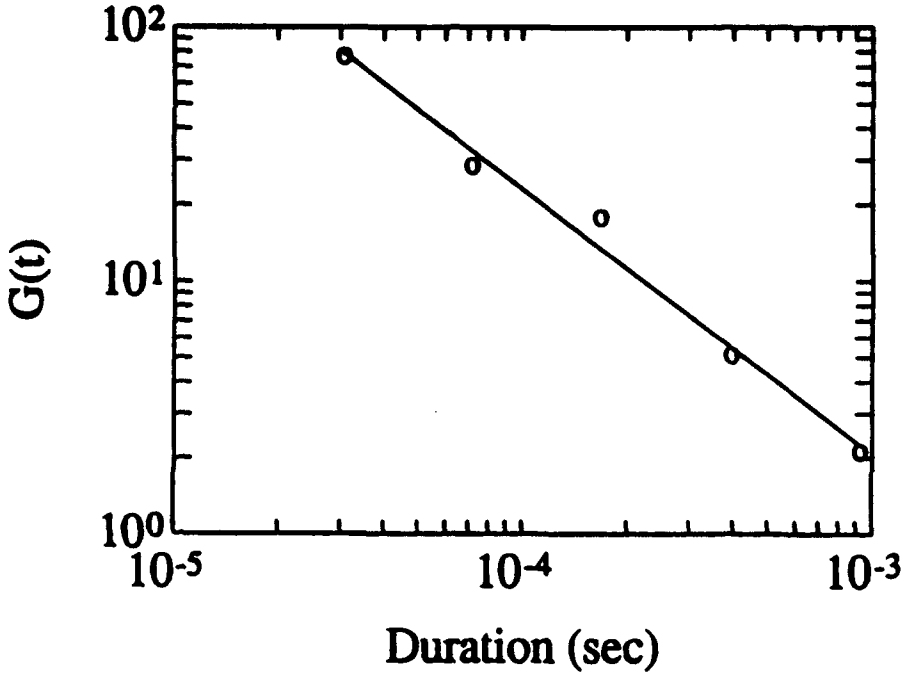

Figure 7. Computed values of the JCF weighted distribution of pulse lifetimes for the train of Figure 3.

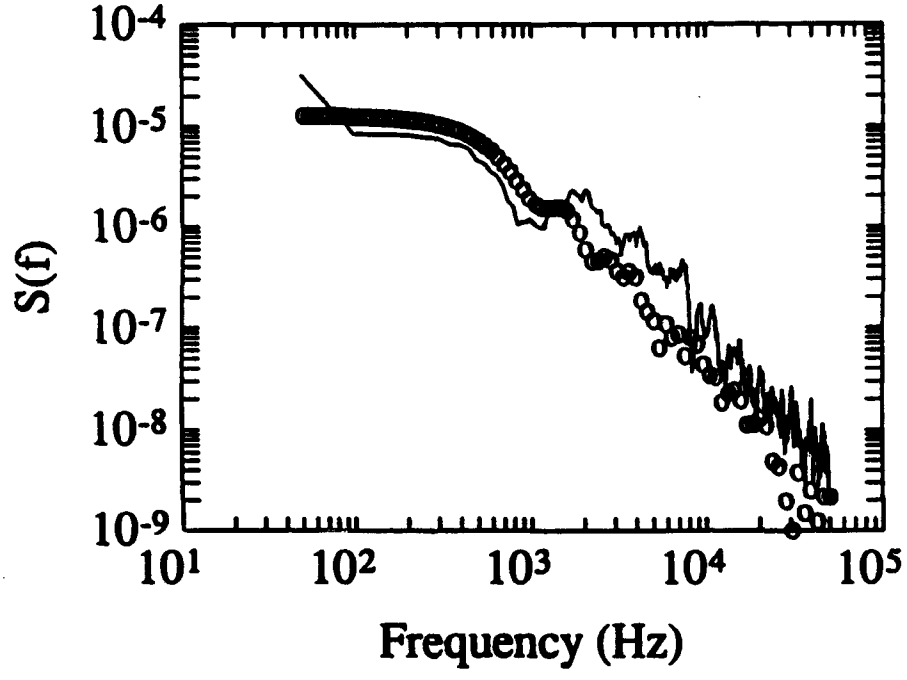

Figure 8. Power spectral density computed from the results of pulse analysis and via FFT of the train of Figure 3.

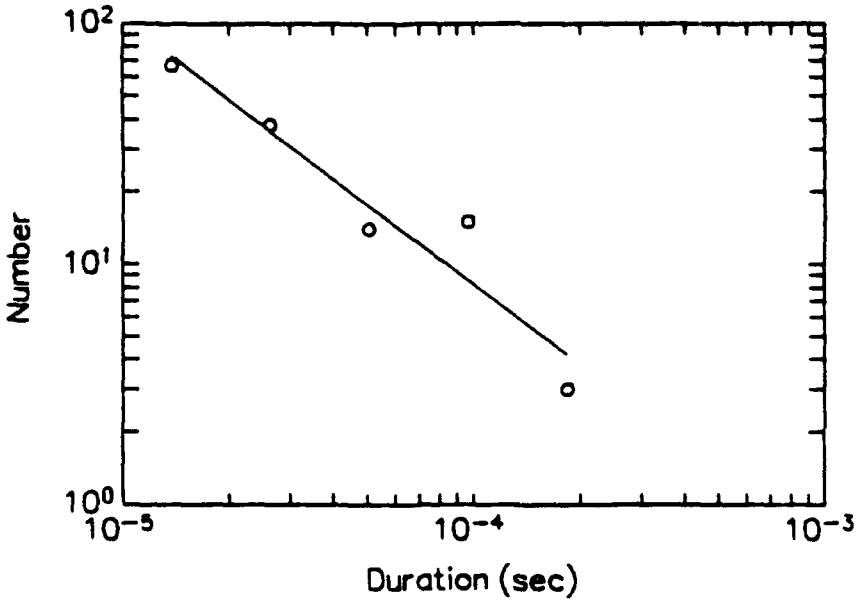

Figure 9. Distribution of durations for a train of 137 Barkhausen pulses in the alumel specimen.

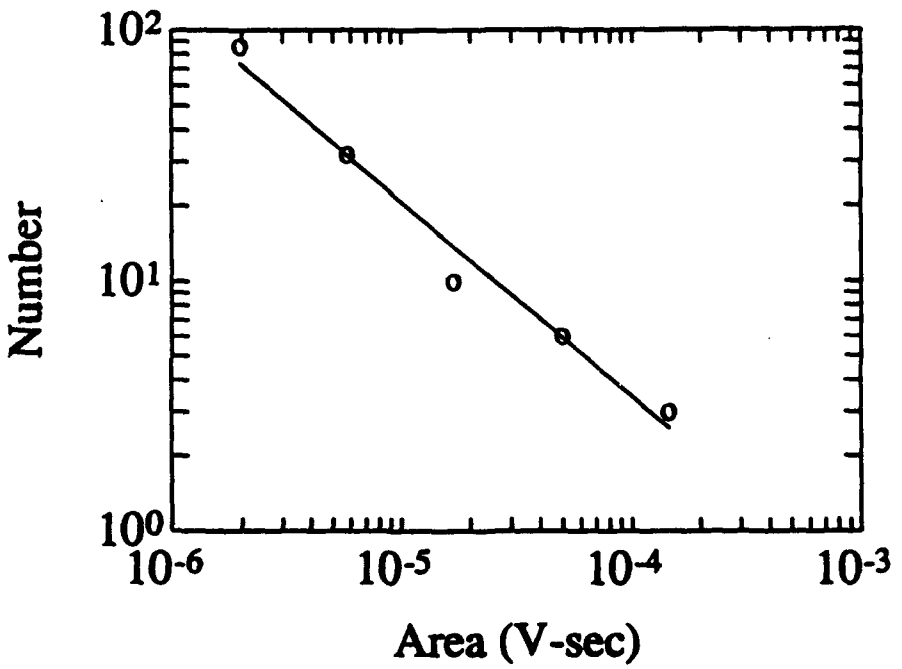

Figure 10. Distribution of areas for the train of Figure 9.

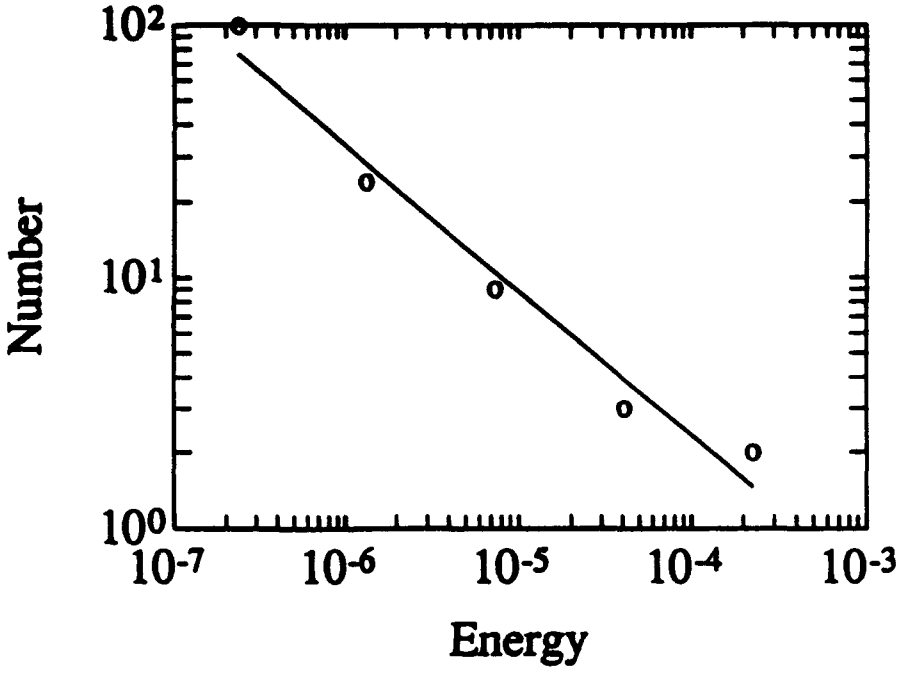

Figure 11. Distribution of energies for the train of Figure 9.

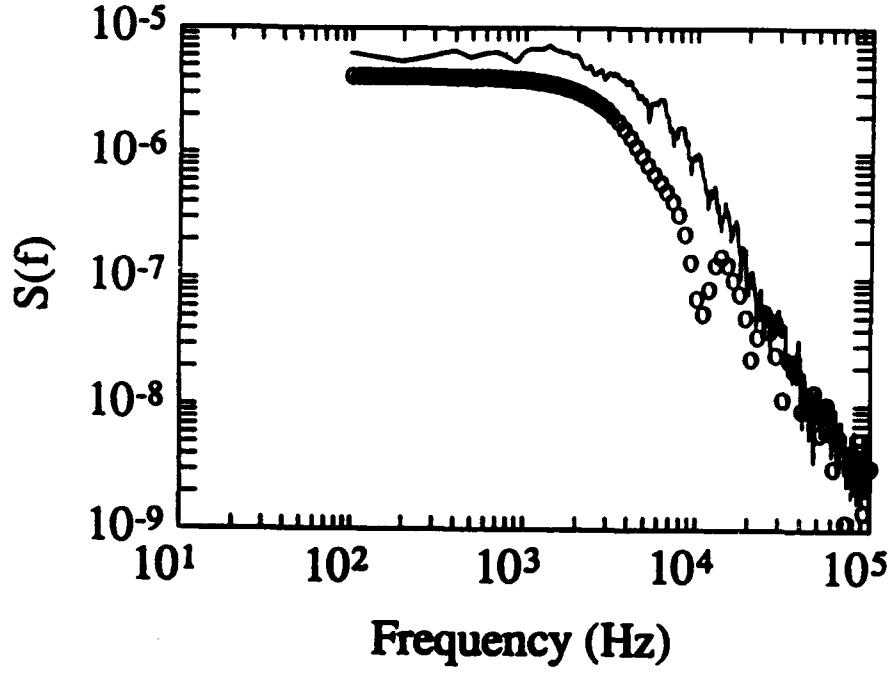

Figure 12. Power spectral density computed from the results of pulse analysis and via FFT of the train of Figure 9.

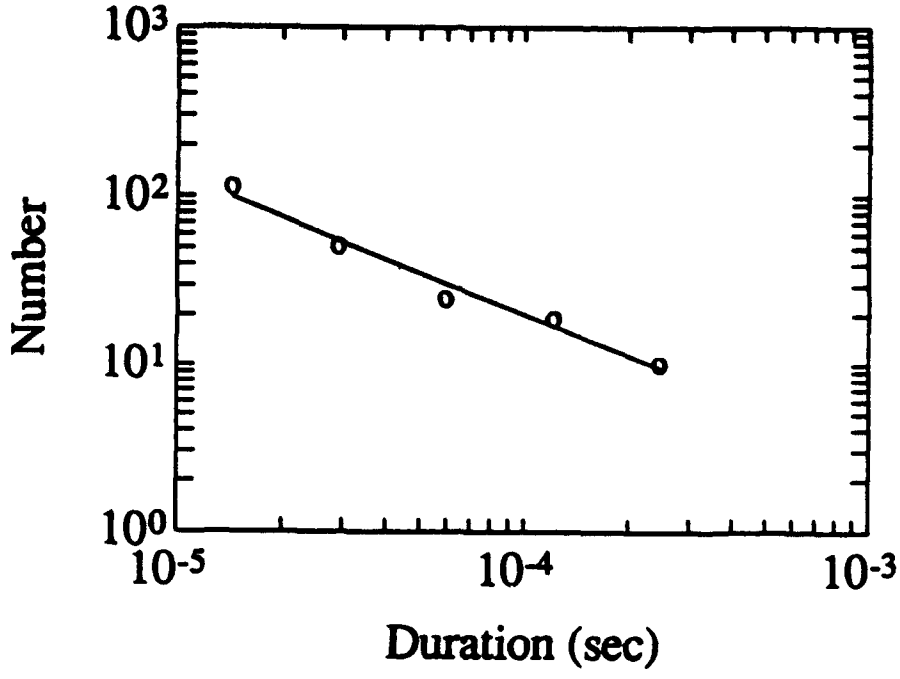

Figure 13. Distribution of durations for a train of 218 Barkhausen pulses in the Metglas specimen.

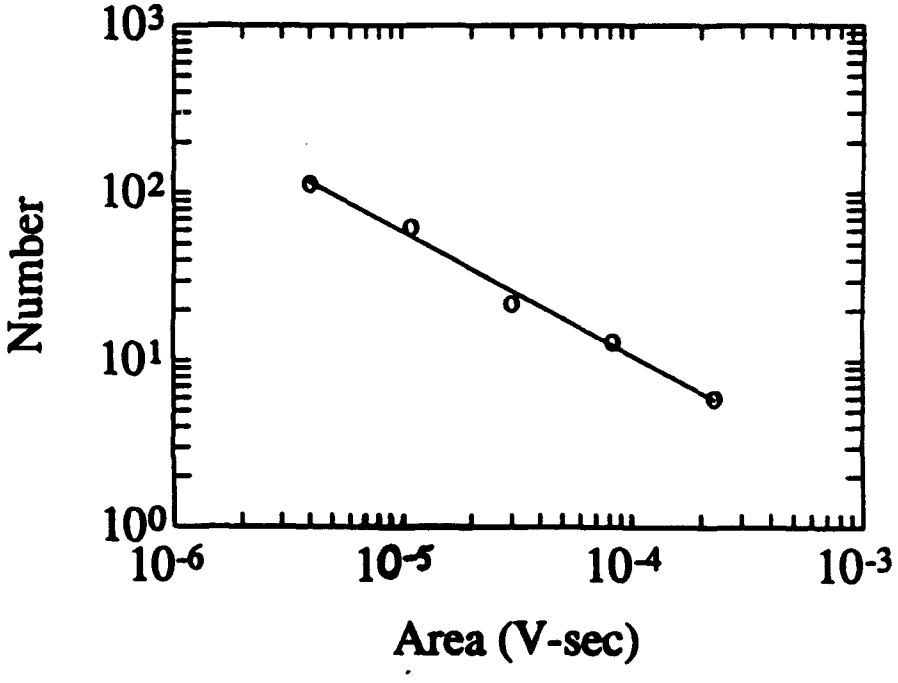

Figure 14. Distribution of areas for the train of Figure 13.

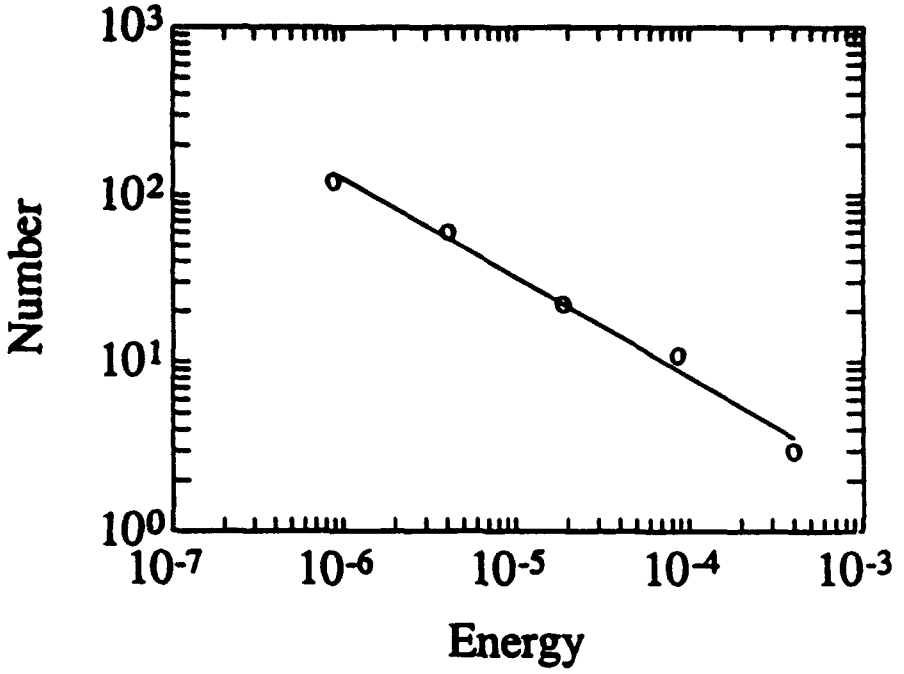

Figure 15. Distribution of energies for the train of Figure 13.

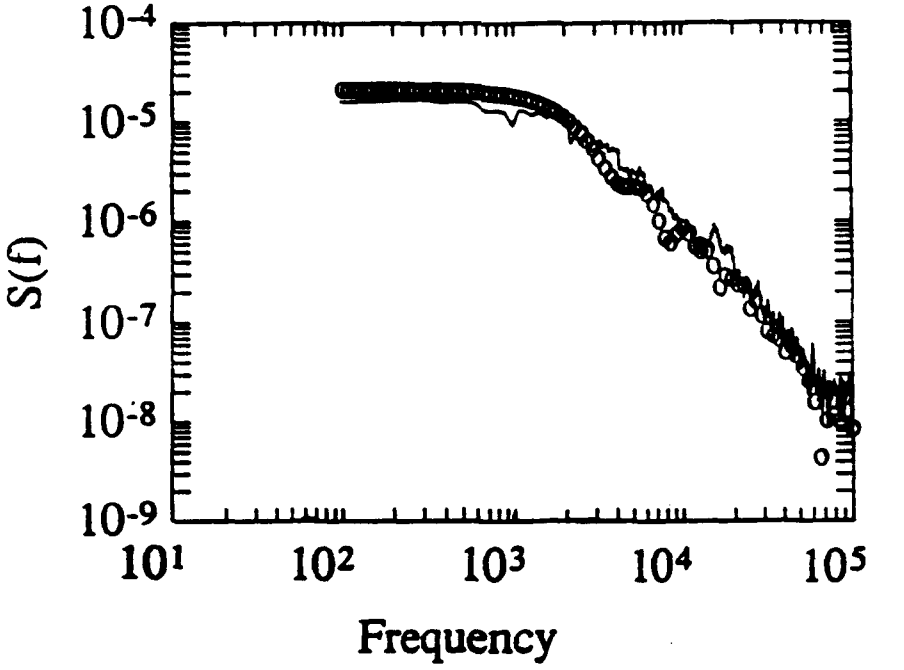

Figure 16. Power spectral density computed from the results of pulse analysis and via FFT of the train of Figure 13.

TECHNICAL REPORT INTERNAL DISTRIBUTION LIST

	NO. OF COPIES
CHIEF, DEVELOPMENT ENGINEERING DIVISION	
ATTN: SMCAR-CCB-DA	1
-DC	1
-DI	1
-DR	1
-DS (SYSTEMS)	1
CHIEF, ENGINEERING SUPPORT DIVISION	
ATTN: SMCAR-CCB-S	1
-SD	1
-SE	1
CHIEF, RESEARCH DIVISION	
ATTN: SMCAR-CCB-R	2
-RA	1
-RE	1
-RM	1
-RP	1
-RT	1
TECHNICAL LIBRARY ATTN: SMCAR-CCB-TL	5
TECHNICAL PUBLICATIONS & EDITING SECTION ATTN: SMCAR-CCB-TL	3
OPERATIONS DIRECTORATE ATTN: SMCWV-ODP-P	1
DIRECTOR, PROCUREMENT DIRECTORATE ATTN: SMCWV-PP	1
DIRECTOR, PRODUCT ASSURANCE DIRECTORATE ATTN: SMCWV-QA	1

NOTE: PLEASE NOTIFY DIRECTOR, BENET LABORATORIES, ATTN: SMCAR-CCB-TL, OF ANY ADDRESS CHANGES.

TECHNICAL REPORT EXTERNAL DISTRIBUTION LIST

	NO. OF COPIES
ASST SEC OF THE ARMY RESEARCH AND DEVELOPMENT ATTN: DEPT FOR SCI AND TECH THE PENTAGON WASHINGTON, D.C. 20310-0103	1
ADMINISTRATOR DEFENSE TECHNICAL INFO CENTER ATTN: DTIC-FDAC CAMERON STATION ALEXANDRIA, VA 22304-6145	12
COMMANDER US ARMY ARDEC	
ATTN: SMCAR-AEE	1
SMCAR-AES, BLDG. 321	1
SMCAR-AET-O, BLDG. 351N	1
SMCAR-CC	1
SMCAR-CCP-A	1
SMCAR-FSA	1
SMCAR-FSM-E	1
SMCAR-FSS-D, BLDG. 94	1
SMCAR-IMI-I (STINFO) BLDG. 59	2
PICATINNY ARSENAL, NJ 07806-5000	
DIRECTOR US ARMY BALLISTIC RESEARCH LABORATORY ATTN: SLCBR-DD-T, BLDG. 305 ABERDEEN PROVING GROUND, MD 21005-5066	1
DIRECTOR US ARMY MATERIEL SYSTEMS ANALYSIS ACTV ATTN: AMXSY-MP ABERDEEN PROVING GROUND, MD 21005-5071	1
DIRECTOR US ARMY RESEARCH LABORATORY ATTN: AMSRL-WT-PD (DR. B. BURNS) ABERDEEN PROVING GROUND, MD 21005-5066	1
COMMANDER ROCK ISLAND ARSENAL ATTN: SMCRI-ENM ROCK ISLAND, IL 61299-5000	1
MIAC/CINDAS PURDUE UNIVERSITY P.O. BOX 2634 WEST LAFAYETTE, IN 47906	1
COMMANDER US ARMY TANK-AUTMV R&D COMMAND ATTN: AMSTA-DDL (TECH LIB) WARREN, MI 48397-5000	1
COMMANDER US MILITARY ACADEMY ATTN: DEPARTMENT OF MECHANICS WEST POINT, NY 10996-1792	1
US ARMY MISSILE COMMAND REDSTONE SCIENTIFIC INFO CTR ATTN: DOCUMENTS SECT, BLDG. 4484 REDSTONE ARSENAL, AL 35898-5241	2
COMMANDER US ARMY FGN SCIENCE AND TECH CTR ATTN: DRXST-SD 220 7TH STREET, N.E. CHARLOTTESVILLE, VA 22901	1
COMMANDER US ARMY LABCOM MATERIALS TECHNOLOGY LAB ATTN: SLCMT-IML (TECH LIB) WATERTOWN, MA 02172-0001	2

NOTE: PLEASE NOTIFY COMMANDER, ARMAMENT RESEARCH, DEVELOPMENT, AND ENGINEERING CENTER, US ARMY AMCCOM, ATTN: BENET LABORATORIES, SMCAR-CCB-TL, WATERVLIET, NY 12189-4050, OF ANY ADDRESS CHANGES.

TECHNICAL REPORT EXTERNAL DISTRIBUTION LIST (CONT'D)

	NO. OF COPIES
COMMANDER US ARMY LABCOM, ISA ATTN: SLCIS-IM-TL 2800 POWDER MILL ROAD ADELPHI, MD 20783-1145	1
COMMANDER US ARMY RESEARCH OFFICE ATTN: CHIEF, IPO P.O. BOX 12211 RESEARCH TRIANGLE PARK, NC 27709-2211	1
DIRECTOR US NAVAL RESEARCH LAB ATTN: MATERIALS SCI & TECH DIVISION	1
CODE 26-27 (DOC LIB)	1
WASHINGTON, D.C. 20375	

	NO. OF COPIES
COMMANDER AIR FORCE ARMAMENT LABORATORY ATTN: AFATL/MN EGLIN AFB, FL 32542-5434	1
COMMANDER AIR FORCE ARMAMENT LABORATORY ATTN: AFATL/MNF EGLIN AFB, FL 32542-5434	1

NOTE: PLEASE NOTIFY COMMANDER, ARMAMENT RESEARCH, DEVELOPMENT, AND ENGINEERING CENTER, US ARMY AMCCOM, ATTN: BENET LABORATORIES, SMCAR-CCB-TL, WATERVLIET, NY 12189-4050, OF ANY ADDRESS CHANGES.